PHYSICAL REVIEW MATERIALS **5**, L030401 (2021)

Letter

# Thermodynamics of boron incorporation in BGaN

Jimmy-Xuan Shen,[1] Mark E. Turiansky,[1] Darshana Wickramaratne,[2,3] and Chris G. Van de Walle[2]

[1]*Department of Physics, University of California, Santa Barbara, California 93106-9530, USA*

[2]*Materials Department, University of California, Santa Barbara, California 93106-5050, USA*

[3]*Center for Computational Materials Science, U.S. Naval Research Laboratory, Washington, DC 20375, USA*

(Received 5 October 2020; accepted 9 February 2021; published 9 March 2021)

We study the thermodynamics of boron (B) incorporation into gallium nitride (GaN) using first-principles calculations. In the dilute limit, we have calculated the formation energies of different configurations of the B impurity in GaN and found that substitution on the cation site is favored over substitution on the anion site. Under *p*-type conditions, interstitial boron can become the more favorable configuration and will ultimately limit the *p*-type conductivity. At higher B concentrations we use the generalized quasi-chemical approximation to elucidate the thermodynamic stability of boron gallium nitride (BGaN) alloys. We also investigate the effects of strain, which will be present if BGaN alloys are grown pseudomorphically on a GaN substrate. Without strain, B incorporation at typical growth conditions is limited to about 1.4% at 800 °C. Pseudomorphic strain raises the limit to 3.0% at the same temperature, close to experimentally observed levels of B incorporation.

DOI: 10.1103/PhysRevMaterials.5.L030401

Alloys of group-III nitrides have enabled the production of commercial light-emitting diodes [1], laser diodes [2], and high-frequency and high-power electronics [3,4]. Ultra-wide-band-gap materials are required to push the wavelength of optoelectronic devices into the ultraviolet range of the spectrum. For transistors, large polarization discontinuities at the interface of III-nitride heterostructures are desirable for enhancing the density of two-dimensional electron gases [5]. Boron nitride (BN) is a promising material for enabling these applications.

BN can be found in the wurtzite, zinc-blende, and layered hexagonal phases. The ground-state polymorph of BN is hexagonal, while the zinc-blende and wurtzite phases are metastable and higher in energy by 60 meV, resp. 90 meV per formula unit [5]. The large difference in the band gap of wurtzite BN and the other III-nitrides [aluminum nitride (AlN), gallium nitride (GaN), and indium nitride (InN)] in principle allows for band-gap engineering across a large range [6–8].

Boron gallium nitride (BGaN) films have been grown using molecular beam epitaxy (MBE) [9–12] and metal organic chemical vapor deposition (MOCVD) [13,14]. Regardless of the growth technique, boron incorporation in these alloys is low, typically less than 5%, and it is unclear whether the alloys are stable against decomposition. Prior first-principles studies have examined the thermodynamics of the zinc-blende phase [15] or the electronic structure [7,8,16,17] of alloys. A study of the thermodynamics of the wurtzite phase is needed, particularly in the regime of low boron concentrations, to shed light on whether the observed alloy concentrations are governed by thermodynamics or kinetics.

When discussing alloying of GaN with other III-nitrides, one tends to implicitly assume substitution on the Ga site. While this is a safe assumption for Al or In, the small size of the B atom renders it possible that B would incorporate on the N site as well. Substitution of B on the N site (an antisite-type impurity) could lead to transition levels in the band gap. Indeed, boron substitution of the nitrogen site ($B_N$) has been proposed for applications in spintronics [18]. However, in the context of alloying GaN with B and the interest in BGaN electronic and optoelectronic devices, there is no information on the relative stability of the different configurations of B in GaN.

We address these fundamental questions about boron incorporation by performing state-of-the-art first-principles calculations to study the thermodynamics of B incorporation in GaN in the dilute limit, as well as at finite concentrations in $B_xGa_{1-x}N$ alloys. In the dilute limit, we find that boron on the gallium site is more likely to incorporate compared to $B_N$, for all values of the Fermi level and under N-poor as well as N-rich conditions. While B incorporation on the N site is found not to occur, we do find that under *p*-type conditions boron is stable as an interstitial and acts as a donor, thus hampering the *p*-type conductivity. Our calculations of the thermodynamics of bulk BGaN alloys show that B incorporation at typical growth conditions is limited to about 1.5%. We also examine the role of strain, assuming pseudomorphic growth on a GaN substrate. We find that by straining the in-plane lattice parameter of BGaN to that of GaN, the upper limit of boron incorporation in BGaN is almost doubled.

Our first-principles calculations are based on density functional theory [19] as implemented in version 5.4 of the VASP code [20,21]. To obtain quantitative accuracy for electronic properties, exchange, and correlation were treated using the hybrid functional of Heyd, Scuseria, and Ernzerhof [22]. The mixing parameter $\alpha$, which determines the amount of exact exchange, was set to 0.29, which produces a band gap of 3.48 eV for GaN, within the range of the experimentally

 ©2021 American Physical Society

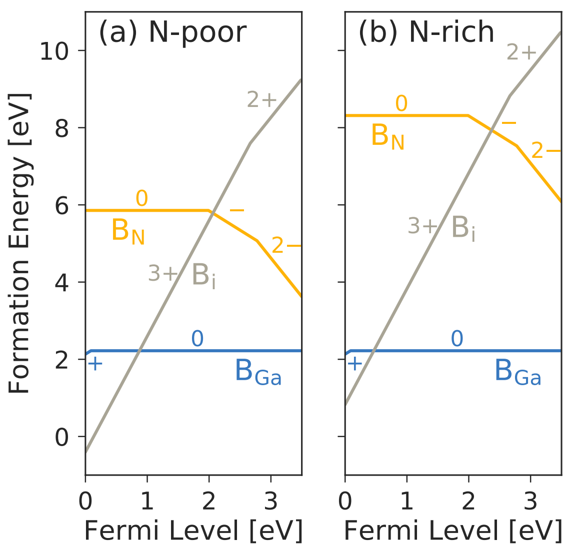


FIG. 1. Formation energies of $B_{Ga}$, $B_N$, and $B_i$ in GaN under (a) N-poor and (b) N-rich conditions.

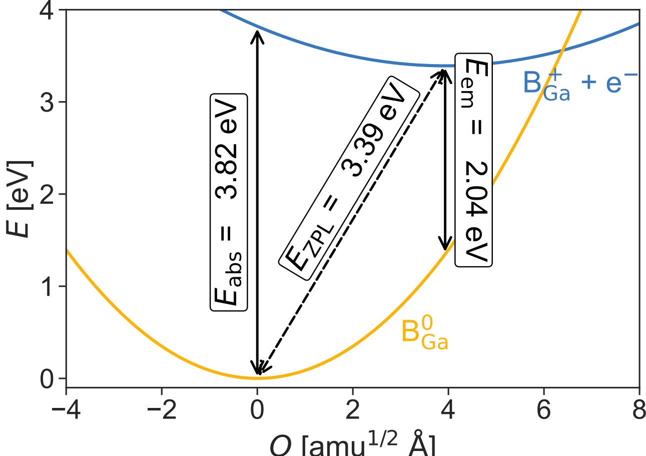


FIG. 2. The configuration coordinate diagram for the (+/0) transition of the $B_{Ga}$ defect. The absorption energy ($E_{abs}$), emission energy ($E_{em}$), and zero-phonon line ($E_{ZPL}$) are shown.

reported values [23]. Projector augmented wave pseudopotentials (with Ga $d$ states included in the core) were used [24] with a cutoff energy of 500 eV. The Brillouin zone of the four-atom unit cell was sampled using a $7 \times 7 \times 4$ $\Gamma$-centered $k$-point grid. Atomic structure relaxations were performed until the forces on each atom were below 5 meV/Å.

To simulate isolated boron impurities in GaN we used a 96-atom supercell, for which a $2 \times 2 \times 2$ $k$-point grid was sufficient for Brillouin-zone integration. Spin polarization was included in the collinear approximation The energy cost to incorporate an impurity $X$ in a solid is the formation energy [25], defined as

$$E^{\mathrm{f}}[X^q] = E_{\mathrm{tot}}[X^q] - E_{\mathrm{tot}}[\mathrm{bulk}] + \sum_i n_i\mu_i + qE_{\mathrm{F}} + \Delta^q \tag{1}$$

where $E_{tot}[X^q]$ is the total energy of the supercell with the impurity in charge state $q$ and $E_{tot}[\text{bulk}]$ is the total energy of the pristine GaN supercell. The chemical potentials $\mu_i$ represent the energy cost of adding ($n_i = -1$) or removing ($n_i = +1$) an atom. The energy cost of adding or removing $q$ electrons to the system is $qE_F$, where $E_F$ is the Fermi level, which is referenced to the valence-band maximum (VBM). Finally, the finite-size charge-state correction $\Delta^q$ was performed using the Freysoldt scheme [25].

We studied B incorporated substitutionally and as an interstitial in GaN. In particular, we investigated the formation energies of boron on the Ga site ($B_{Ga}$) or on the N site ($B_N$), and boron in an interstitial site ($B_i$). The chemical potential $\mu_N$ can vary between N-rich (equilibrium with $N_2$) or N-poor conditions (equilibrium with metallic Ga). For the chemical potential of boron, $\mu_B$, the range is determined by the limiting phase, for which we chose wurtzite BN.

The formation energies [Eq. (1)] of various configurations of boron impurities in GaN are shown in Fig. 1. The formation energies of $B_{Ga}$ are identical under N-poor and N-rich conditions; this can be easily shown by inserting expressions for $\mu_B$ and $\mu_{Ga}$ under N-poor and N-rich conditions into Eq. (1).

For almost all values of the Fermi level, $B_{Ga}$ is the most stable configuration for boron to be incorporated, and it is stable mainly in the neutral charge state. This is reassuring from the point of view of growth of BGaN alloys, which is based on an expectation of isovalent substitution. $B_{Ga}$ is stable in a positive charge state over a very small range of Fermi levels near the VBM; the (+/0) charge-state transition level occurs at 0.09 eV. The atomic configuration of the + charge state corresponds to a hole polaron on a N neighbor of the B impurity, with B moving into the plane of its other N neighbors. The presence of the (+/0) transition offers a way to detect the presence of $B_{Ga}$ in optical experiments. The optical transitions attributed to the $B_{Ga}$ defect are shown in Fig. 2. Because of the large difference in lattice relaxations between the + and 0 charge states, the photoluminescence line will be broad, with a peak that is significantly shifted from the zero-phonon line at $3.48 - 0.09 = 3.39$ eV; our calculations indicate this peak occurs at 2.04 eV.

$B_N$ can occur in the neutral, −, and 2− charge state, i.e., as expected it acts as a (deep) double acceptor. However, it has significantly higher formation energies than $B_{Ga}$ for all values of the Fermi level and all chemical potentials, and hence it is highly unlikely to form.

For the boron interstitial, we explored various possible initial positions, but found it to be most stable at a site near the octahedral interstitial site; this site is in the hexagonal channel, equidistant from six Ga and six N atoms. The final stable site was found to be very close to the O′ site shown in Fig. 5 of Ref. [26], which was the stable site for a $Be_i^{2+}$ interstitial. The boron interstitial also has a fairly high formation energy for most Fermi levels and will not incorporate under $n$-type conditions. But since it acts as a triple donor, its formation energy (in the 3+ charge state) becomes very low for Fermi-level positions close to the VBM. Growth of $p$-type BGaN alloys will thus be hampered by the preferential incorporation of B on interstitial sites.

Boron is a significantly smaller atom than Ga, and the incorporation of B on the Ga site leads to a symmetric inward displacement of the nearest-neighbor N atoms, by 15%

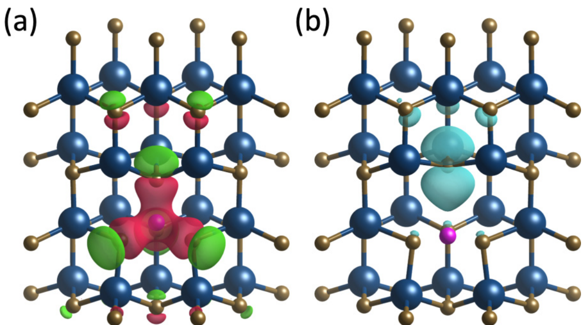


FIG. 3. (a) The atomic configuration of the $B_{Ga}$ impurity in the neutral charge state, along with the change in charge density (as defined in the text). Ga atoms are shown in blue, N in gold, and B in magenta. The red isosurface bounds a region of increased charge, and the green isosurface a region of decreased charge. (b) The atomic configuration of the $B_{Ga}$ impurity in the positive charge state. An isosurface of the polaronic state is shown in cyan.

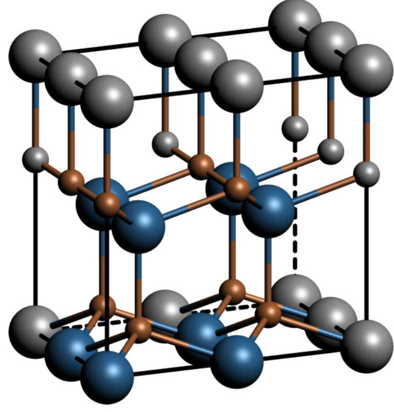

FIG. 4. Sixteen-atom cluster of the wurtzite nitride structure. The gold sites represent the nitrogen atoms, and the blue cation sites can be occupied by either a B or Ga atom. Periodic images of atoms are shown in gray.

of the Ga-N bond length (1.95 Å). The shorter B-N bond length in BN (1.56 Å) indicates a stronger bond between B and N than between Ga and N. Indeed, the B–N bond is one of the strongest in nature. This difference in bond strengths is evident in the difference in charge densities between the $B_{Ga}$ impurity and the pristine GaN as shown in Fig. 3(a). The amount of distortion around $B_{Ga}$ is consistent with force-model predictions for tetrahedral-site substitutions in the dilute limit [27]. In Fig. 3(b) we show the atomic configuration of the positive charge state, where B has moved into the plane of three N neighbors, and a hole polaron is present on the N neighbor along the $c$ axis.

We have established that the cation substitution ($B_{Ga}$) is the most likely configuration of the B impurity in GaN. Now we turn to studying the solubility limit of B incorporation in GaN, which requires careful treatment of the mixing entropy. To model BGaN solid solutions we use the generalized quasi-chemical approximation (GQCA) [28], in which the wurtzite alloy is approximated as an ensemble of independent clusters. These clusters are represented by $2 \times 2 \times 1$ supercells containing 16 atoms with the structure shown in Fig. 4.

The eight cation sites in the 16-atom wurtzite cluster can be occupied by either a Ga or B atom. Hence, there are $2^8 = 256$ different configurations that can be reduced to $J = 22$ distinct cluster classes by symmetry operations [29]. In the GQCA framework, the crystal is treated as a large ensemble of $M$ clusters, with $M_j$ clusters from each class. The fraction of a given cluster class is $x_j = \frac{M_j}{M}$ for $j = 0, \ldots, J$, and any physical quantity that is a function of the alloy concentration ($x$) and temperature ($T$) can be expressed as a function of the $x_j$'s. Each $x_j$ thus has an implicit dependence on $x$ and $T$. The total energy of each cluster is denoted by $\varepsilon_j$ and the excess energy $\Delta_j$ is given by

$$\Delta_j = \varepsilon_j - \left(\frac{m - m_j}{m}\varepsilon^s_{\mathrm{GaN}} + \frac{m_j}{m}\varepsilon^s_{\mathrm{BN}}\right), \tag{2}$$

where $m_j$ is the number of boron atoms (out of the $m \equiv 8$ cation sites) in that cluster, $\varepsilon^s_{\mathrm{GaN}}$ is the energy of a cluster with only Ga cations, and $\varepsilon^s_{\mathrm{BN}}$ is the energy of a cluster with only B cations. The term in parentheses in Eq. (2) therefore represents a linear interpolation between the "pure GaN" and the "pure BN" cases. Note that the pure cluster energies $\varepsilon^s_{\mathrm{GaN}}$ and $\varepsilon^s_{\mathrm{GaN}}$ can differ from the equilibrium bulk energies of the binary end compounds $\varepsilon_{\mathrm{GaN}}$ and $\varepsilon_{\mathrm{BN}}$ if strain is included by modifying the lattice parameters [28]; hence the use of the superscript "s." For the unstrained case, the shape and atomic configuration of each of the 22 inequivalent clusters were allowed to relax while for the strained case the in-plane lattice parameters were fixed to those of GaN.

We can determine the cluster fraction as a function of $x$ and $T$, $x_j(x, T)$, by minimizing the Gibbs free energy of mixing $\Delta G(x, T)$ with respect to the $x_j$'s. For solid solutions, the $P\Delta V$ term is small, so the difference between the Gibbs and Helmholtz free energies can be neglected. The Helmholtz free energy of mixing, $\Delta F(x, T)$, is given by

$$\Delta F(x, T) = \Delta U(x, T) - T\Delta S(x, T), \tag{3}$$

where $\Delta U(x, T)$ is the mixing enthalpy and $\Delta S(x, T)$ is the mixing entropy. For the $M$ clusters with $m$ sites, the mixing enthalpy is given by

$$\begin{aligned}\Delta U(x, T) = M[(1 - x)(\varepsilon^s_{\mathrm{GaN}} - \varepsilon_{\mathrm{GaN}}) + x(\varepsilon^s_{\mathrm{BN}} - \varepsilon_{\mathrm{BN}})] \\ + M\sum_j x_j\Delta_j\,;\end{aligned} \tag{4}$$

and the mixing entropy is given by

$$\begin{aligned}\Delta S(x, T) = -Nk_B[x\ln x + (1 - x)\ln(1 - x)] \\ - Mk_B\sum_j x_j \ln\left(\frac{x_j}{x^0_j}\right),\end{aligned} \tag{5}$$

where $k_B$ is Boltzmann's constant and

$$x^0_j = g_j(1 - x)^{(m - m_j)}x^{m_j} \tag{6}$$

is the cluster fraction in a random alloy [28] and $g_j$ is the degeneracy of the cluster with energy $\varepsilon_j$. Since $\Delta U$ and $\Delta S$ can both be expressed in terms of the cluster fractions $x_j$, for a given point in the phase space $(x, T)$ the free energy can be minimized with respect to the $x_j$'s to obtain $\Delta F(x, T)$ and $x_j(x, T)$.

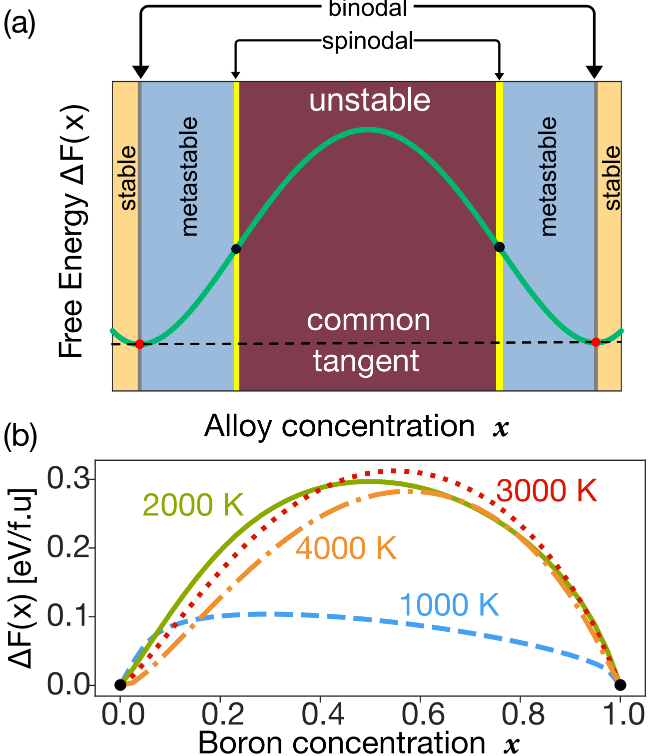


FIG. 5. (a) Schematic of the free energy, at a given temperature, as a function of the alloy concentration $x \in [0, 1]$. The end points $[\Delta F(0), \Delta F(1)]$ are both zero by definition. Between the binodal boundary points, the solid solution can globally lower the free energy by decomposing into two different phases. Between the spinodal points, the solid solution is locally unstable against decomposition. The inflection points mark the limits of spinodal decomposition. (b) $\Delta F(x)$ curves for unstrained BGaN alloys calculated using the GQCA at various temperatures. Note that the stable region is negligibly small.

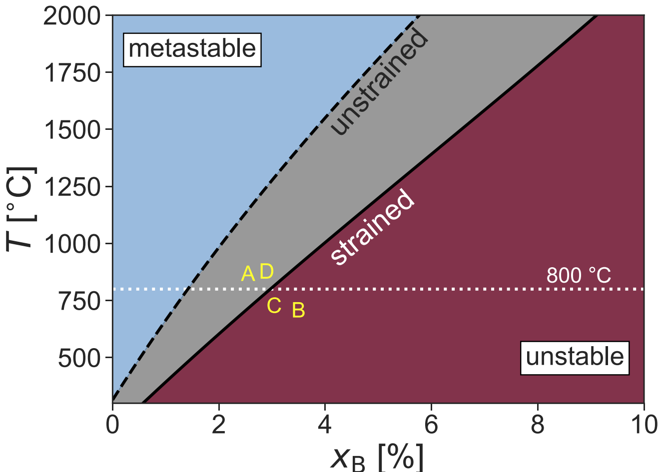


FIG. 6. Phase diagram of BGaN alloys obtained using the GQCA approach. The spinodal boundary of bulk BGaN is shown with the dashed line, while the spinodal boundary of BGaN strained to the in-plane lattice constant of GaN is shown with the solid line. The experimental limits of B incorporation are shown as reported in the following studies: (A) Vezin *et al.* [9], (B) Williamson *et al.* [10], (C) Cramer *et al.* [11], and (D) Malinauskas *et al.* [14].

Using this formalism, we obtained the free energy [Eq. (3)] at different temperatures. The approach is similar to Ref. [30], but with particular attention to calculating spinodal boundaries and incorporating effects of strain. At a given temperature, the *binodal* points are determined by the common tangent points in the free energy curve (see Fig. 5). Between the binodal points, the alloy can globally lower its free energy by decomposing into two distinct phases. Between the *spinodal* points, where $\frac{\partial^2}{\partial x^2}\Delta F = 0$, the material will locally spontaneously decompose and the alloy cannot be grown at all. In the region between the binodal and spinodal points, the material is metastable and can be grown under certain conditions.

The mixing enthalpy of BGaN is positive, as we expect in an isovalent alloy. The large difference in the natural bond lengths of the B–N and Ga–N bonds causes the mixing enthalpy to be larger than in traditional nitride alloys. The calculated free energy is dominated by the positive enthalpy term $(\Delta U)$ from Eq. (1). We find that, below the melting point of GaN (2538 °C [31]), $\Delta F$ is positive over the entire range of boron concentrations. A positive free energy at all $x$ means that the free energy of $B_xGa_{1-x}N$ can always be lowered globally by decomposing into GaN and BN. Figure 5(b) indeed shows that the $\Delta F$ curves do not exhibit any binodal-type stability, even at temperatures well beyond the melting point of GaN. Hence, the solid solution will always decompose under equilibrium conditions. However, the material can still be grown using nonequilibrium growth methods such as MBE, since it is stable against local decomposition up to the spinodal boundary. Between the binodal and spinodal boundaries, the curvature of the free energy $\frac{\partial^2}{\partial x^2}\Delta F$ is positive. For any boron concentration $x$ in this range, the free energy is lower than the average free energy for two values close to $x$, so the alloy will not locally decompose. In the metastable region, the material can decompose only by nucleation and growth of the second phase.

The phase diagram in Fig. 6 shows how the spinodal transition point changes as a function of temperature. Here temperatures are reported in degrees Celsius for easier comparison with experiment, where those units are commonly used. To identify the limit for boron incorporation in GaN we examine temperatures up to 2000 °C, paying particular attention to the temperature range between 750 and 1000 °C that is representative of temperatures in MBE [11] and MOCVD [14] growth of BGaN alloys. At 800 °C, we find a limit of 1.4% B incorporation for unstrained alloys; for strained alloys, this limit is increased to 3.0%.

In Fig. 6 we also show experimental results for the maximum concentration of boron that could be incorporated in the alloy at a given temperature [9–11,14]. We observe that our calculated spinodal boundary for the case where strain is included agrees well with the experimentally obtained limits. Our calculations indicate that it will not be possible to overcome the experimentally observed limits on boron incorporation; increasing the B concentration triggers spinodal decomposition, which will spontaneously occur regardless of the growth conditions.

An important conclusion from our calculations is that strain has an important effect on the stability of the alloy, with the stability boundary being shifted to significantly higher boron concentrations in the presence of tensile strain. Based on this finding, we suggest that growing on substrates with a larger lattice parameter than GaN could potentially lead to higher boron incorporation.

In summary, we have examined various aspects of the thermodynamics of B incorporation into GaN. In the dilute limit we showed that B preferentially substitutes on the Ga site. However, for *p*-type conditions, the interstitial B impurity (which acts as a donor) is the preferred configuration, which will suppress incorporation on substitutional sites and also compensate *p*-type conductivity. For the BGaN alloys we have examined the limits of B incorporation for unstrained alloys as well as for films strained to match the lattice parameters of GaN. We find that B can incorporate into GaN at significantly higher concentrations in the strained case. Overall, however, the fundamental limit on B incorporation into GaN is still relatively low.

We thank J. S. Speck for fruitful discussions and feedback. J.-X.S. was supported by the National Science Foundation (NSF) under Grant No. DMR-1434854. M.E.T. was supported by the National Science Foundation (NSF) MRSEC program (DMR-1720256). Work by D.W. on boron defects in GaN was supported by the U.S. Department of Energy (DOE), Office of Science, Basic Energy Sciences (BES), under Award No. DE- SC0010689, and work on BGaN alloys was supported by a National Research Council Fellowship at the U.S. Naval Research Laboratory. Computational resources were provided by the Extreme Science and Engineering Discovery Environment (XSEDE), supported by NSF (ACI-1548562).

[1] S. Nakamura and M. R. Krames, Proc. IEEE **101**, 2211 (2013).
[2] A. Pourhashemi, R. M. Farrell, D. A. Cohen, J. S. Speck, S. P. DenBaars, and S. Nakamura, Appl. Phys. Lett. **106**, 111105 (2015).
[3] U. Mishra, P. Parikh, and Yi-Feng Wu, Proc. IEEE **90**, 1022 (2002).
[4] V. Ravindran, M. Boucherit, A. Soltani, S. Gautier, T. Moudakir, J. Dickerson, P. L. Voss, M.-A. di Forte-Poisson, J.-C. De Jaeger, and A. Ougazzaden, Appl. Phys. Lett. **100**, 243503 (2012).
[5] C. E. Dreyer, J. L. Lyons, A. Janotti, and C. G. Van de Walle, Appl. Phys. Express **7**, 031001 (2014).
[6] A. Ougazzaden, S. Gautier, T. Moudakir, Z. Djebbour, Z. Lochner, S. Choi, H. J. Kim, J.-H. Ryou, R. D. Dupuis, and A. A. Sirenko, Appl. Phys. Lett. **93**, 083118 (2008).
[7] J.-X. Shen, D. Wickramaratne, and C. G. Van de Walle, Phys. Rev. Mater. **1**, 065001 (2017).
[8] M. E. Turiansky, J.-X. Shen, D. Wickramaratne, and C. G. Van de Walle, J. Appl. Phys. **126**, 095706 (2019).
[9] V. Vezin, S. Yatagai, H. Shiraki, and S. Uda, Jpn. J. Appl. Phys. **36**, L1483 (1997).
[10] T. L. Williamson, N. R. Weisse-Bernstein, and M. A. Hoffbauer, Phys. Status Solidi C **11**, 462 (2014).
[11] R. C. Cramer, B. Bonef, J. English, C. E. Dreyer, C. G. Van de Walle, and J. S. Speck, J. Vac. Sci. Technol. A **35**, 041509 (2017).
[12] B. Bonef, R. Cramer, and J. S. Speck, J. Appl. Phys. **121**, 225701 (2017).
[13] A. Y. Polyakov, M. Shin, M. Skowronski, D. W. Greve, R. G. Wilson, A. V. Govorkov, and R. M. Desrosiers, J. Electron. Mater. **26**, 237 (1997).
[14] T. Malinauskas, A. Kadys, S. Stanionytė, K. Badokas, J. Mickevičius, J. Jurkevičius, D. Dobrovolskas, and G. Tamulaitis, Phys. Status Solidi B **252**, 1138 (2015).
[15] L. K. Teles, L. M. R. Scolfaro, J. R. Leite, J. Furthmüller, and F. Bechstedt, Appl. Phys. Lett. **80**, 1177 (2002).
[16] M. B. Kanoun and S. Goumri-Said, Semicond. Sci. Technol. **23**, 125036 (2008).
[17] L. Escalanti and G. L. W. Hart, Appl. Phys. Lett. **84**, 705 (2004).
[18] S. W. Fan, X. N. Huang, and K. L. Yao, J. Appl. Phys. **121**, 073905 (2017).
[19] W. Kohn and L. J. Sham, Phys. Rev. **140**, A1133 (1965).
[20] G. Kresse and J. Furthmüller, Phys. Rev. B **54**, 11169 (1996).
[21] G. Kresse and J. Furthmüller, Comput. Mater. Sci. **6**, 15 (1996).
[22] J. Heyd, G. E. Scuseria, and M. Ernzerhof, J. Chem. Phys. **124**, 219906 (2006).
[23] O. Madelung, *Semiconductors: Data Handbook* (Springer Science & Business Media, Berlin, 2012).
[24] P. E. Blöchl, Phys. Rev. B **50**, 17953 (1994).
[25] C. Freysoldt, B. Grabowski, T. Hickel, J. Neugebauer, G. Kresse, A. Janotti, and C. G. Van de Walle, Rev. Mod. Phys. **86**, 253 (2014).
[26] C. G. Van de Walle, S. Limpijumnong, and J. Neugebauer, Phys. Rev. B **63**, 245205 (2001).
[27] C. K. Shih, W. E. Spicer, W. A. Harrison, and A. Sher, Phys. Rev. B **31**, 1139 (1985).
[28] A.-B. Chen and A. Sher, *Semiconductor Alloys: Physics and Materials Engineering* (Plenum Press, New York, 1995).
[29] A. Schleife, M. Eisenacher, C. Rödl, F. Fuchs, J. Furthmüller, and F. Bechstedt, Phys. Rev. B **81**, 245210 (2010).
[30] F. Brivio, C. Caetano, and A. Walsh, J. Phys. Chem. Lett. **7**, 1083 (2016).
[31] K. Harafuji, T. Tsuchiya, and K. Kawamura, J. Appl. Phys. **96**, 2501 (2004).